Physics Letters A 426 (2022) 127889

Contents lists available at ScienceDirect

Physics Letters A

www.elsevier.com/locate/pla

Late dynamics of large-scale vortices in periodic two-dimensional flows

J. Chai [a,b,c], L. Fang [c,d,*]

[a] Institute of Mechanics, Chinese Academy of Sciences, Beijing 100190, China
[b] School of Engineering Science, University of Chinese Academy of Sciences, Beijing 100049, China
[c] Laboratory of Complex Systems, Ecole Centrale de Pékin, Beihang University, Beijing 100191, China
[d] Beihang Hangzhou Innovation Institute Yuhang, Hangzhou 310023, China

ARTICLE INFO

Article history:
Received 14 August 2021
Received in revised form 11 November 2021
Accepted 7 December 2021
Available online 13 December 2021
Communicated by A. Das

Keywords:
Homogeneous isotropic turbulence
Two-dimensional turbulence
Point vortex
Direct numerical simulation

ABSTRACT

The inverse cascade in freely decaying two-dimensional flows with periodic boundary conditions will lead to a quasi-steady long-term system of vortices, which has not been well investigated in literature. By performing a series of direct numerical simulations, we focus on the late dynamics of these large-scale vortices. It is found that the theories of point vortices can be also approximately employed for both quadrate and hexagonal periodic conditions, however, in real flows the dynamics can switch among different motions, which differs from the theory of point vortices. It is observed as a special case of the wandering motions that the weakest vortex can migrate among different periods, with the other two vortices co-rotating. This phenomenon can be analogical to the physics of current flow. In addition, the merging procedure of large-scale vortices can be described by using the skewness of vorticity.

1. Introduction

In two-dimensional (2D) turbulence, dual cascade exists, indicating that energy transfers towards both large and small scales [1, 2]. A direct consequence of the inverse energy transfer is that the vortices will merge, and finally there will be a quasi-steady long-term system of vortices (see *e.g.*, Fig. 2 of Ref. [3]). The dynamics of the vortices, including the merging and motions, is an interesting research topic and has attracted many studies.

Before the quasi-steady state, kinetic energy exists at all scales, which implies that the flow contains lots of vortices at different scales. Existing studies for the dynamics of these vortices were usually based on statistical tools. It has been often proposed [4–7] that the statistical equilibria of interacting point vortices can be used to interpret 2D turbulence. Equilibrium statistics of a cluster of a large number of positive 2D point vortices in an infinite region were studied analytically and numerical cases were performed to verify the equilibrium configurations [5]. The non-equilibrium situation caused by a weak external velocity field has also been studied in which the negative viscosity effect that describes the increase of size and decrease of their displacement for interacting clusters arised [5]. Reference [8] showed that the interacting vortices and the spin-up phenomenon in a rigid container can be interpreted in terms of these statistical models. Other studies have been performed to investigate more general vortices with a typical size instead of a cluster of point vortices. Mcwilliams [9] discussed the criteria of identification of vortex and proposed a procedure of vortex census from numerical results. The statistical characteristics such as the distribution of the density or population, size, and radial profile of the coherent vortices that dominate the two-dimensional freely evolving turbulence were analyzed and interpreted [9]. The evolution of density was found to be decaying. A scaling theory expressing the statistical properties in terms of one parameter was then proposed and supported by numerical simulations and solutions of a modified point-vortex model [10]. In Ref. [11], a scale-invariant behavior corresponding to the self-similar scaling of compensation between density and mean vortex intensity was found. In addition, geometrical structures and amount of coherent vortices generated by inverse cascade of 2D turbulence in a finite box was discussed in Ref. [12]. It was also proved theoretically in Ref. [13] that 2D decaying turbulence field with integrable initial vorticity distribution converges to the Oseen vortex solution, which is coherent with the experimental and numerical observation of inverse energy cascade and form of large-scale vortex structures [14].

There have been also investigations focusing on the merging procedure of several 2D vortices. The interaction and instability of a vortex pair has been studied in experiments for investigating three-dimensional elliptic instability of a counter-rotating vortex

* Corresponding author.
E-mail address: le.fang@zoho.com (L. Fang).

https://doi.org/10.1016/j.physleta.2021.127889
0375-9601/

pair to short waves [15] and the numerical studies on how coexisting the vertical shear and stratification affect the evolution of a vortex pair [16] were given. Elliptic short-wave instability was also found to be important in the merging process of co-rotating vortices, in configurations similar to those found in the extended near-wake of typical transport aircraft [17]. Experiments, numerical cases and theoretical studies illustrated phenomena such as earlier merging and larger final vortex core [17]. In Ref. [17], the theoretical analysis was based on the point-vortex assumption. In 2D flows, vortex merging is the principal ingredient of the inverse cascade [9,14,18]. The numerical and theoretical study of merging of a vortex pair were also performed in previous study such as how the Reynolds number affects each of the three phases that characterize this phenomenon [19].

To our knowledge, there is no systematic investigation about the late dynamics of large-scale vortices in 2D flows (an example can be Fig. 2b of Ref. [3], where the flow finally evolves to two vortices). In Refs. [9–11], the evolution of vortex in 2D flows was investigated in a statistical way and they concentrated on a relatively early stage with a great number of vortices. Obviously, the scale of these vortices will be comparable to the size of computational domain, indicating that the boundary condition can be important for the late dynamics of large-scale vortices. Aiming at generating homogeneous isotropic flows, the most common method is to use periodic conditions in a cube, but we can also introduce periodic conditions in a hexagon [20]. From Fig. 11 of Ref. [20] it can be observed that different periodic conditions affect the late evolution of large-scale energies, but it is still unclear how they affect the late dynamics of large-scale vortices.

If we approximately consider the large-scale vortices as point vortices, analytical results can be found in literature. We refer to Ref. [21] as a comprehensive review. Some studies focused on the stationary configurations of point vortices in an unbounded region [22,23], as well as their instability properties [24,25]. Reference [26] extracted the motion of three-vortex system with zero total circulation near equilibrium position using asymptotic analysis. For the nonstationary configurations, the problem of motion can be translated to a Hamiltonian dynamical system, which is usually nonintegrable for four and more point vortices [27]. Analytical researches then focused on three vortices system [28–30]. Considering the periodic boundary conditions, Ref. [31] also provided a detailed analytical analysis on the motion of three point vortices. Typical cases of three point vortices system in unbounded domain with an opposite-signed vortex pair and a fixed vortex has been widely studied. It was pointed out that the entrapping of the vortex pair can be predicted only by calculating two parameters which are the ratio of distances to the fixed vortex and the ratio of strengths [32–34]. In addition, Aref [31] noted that simply changing the shape of periodic parallelogram that contains three point vortices introduces new qualitative behavior, leading to possible implications for numerical simulations of 2D turbulence which are conducted traditionally with quadrate periodic conditions. However, it is still not clear whether these results for point vortices can be used to real 2D flows.

In brief, systematic investigation about the late dynamics of large-scale vortices in 2D flows is still lack. The effects of different periodic conditions are not clear, and the applicability of the point-vortex theories is needed to be verified. In the present contribution we will perform numerical simulations by using the algorithms introduced in Ref. [20], to clarify these questions and to reveal new phenomena.

Table 1
Number the cases with different long-term categories.

	Hexagonal Cases	Cartesian Cases
Two-vortices	46 cases	41 cases
Three-vortices	13 cases	17 cases
Three-vortices to Two-vortices	12 cases	22 cases
Four-vortices to Two-vortices	9 cases	0 case

2. Descriptions of problem

2.1. General descriptions

As introduced in the previous section, during the evolution of 2D turbulence, the condensation of all the vorticities into several large-scale vortices can be observed in long time. When an isotropic freely decaying turbulent field is generated by introducing quadrate periodic boundary conditions in two directions of coordinate axis, the most frequent observation is the formation of a two-vortices system in a periodic square. Fig. 1 is an example of the initial vorticity field in a direct numerical simulation (DNS) case and of the two-vortices structure after long time evolution. Dashed lines indicate the periodic boundaries. A characteristic length L, defined from the minimal distance $\Delta_k = 2\pi/L$ between the wavenumbers in spectral space (see Fig. 1 of Ref. [20] as a sketch), is used for normalization. Another example can be found in Fig. 2 of Ref. [3]. The dynamics of the two-vortices structure is simply a uniform rigid translation motion, therefore it can be considered as trivial.

Besides the two-vortices system, in practice we also observe other types of large-scale vortices for long time. As an example, in Fig. 2(a) we show that the flow can evolve to a quasi-stable three-vortices coherent structure in a period. The values of vorticity or strength of these three vortices are two positive and one negative, respectively. Their trajectories are shown in Fig. 2(b). As will be analyzed in the following parts, this kind of motion is the paired motion. In Fig. 3, we show that the three-vortices coherent structure can also occur under hexagonal periodic conditions (dashed lines indicate the periodic boundaries). Due to the complexity of dynamics, we will focus on the dynamics of these vortices systems in the following parts.

2.2. Descriptions of DNS cases

The evolution of 2D freely decaying turbulence is computed using pseudo-spectral Fourier code in a stream-vorticity formulation. Detailed information on the in-house code can be found in Ref. [3]. The initial field is generated by using the Rogallo method [35]. Two groups of DNS cases are performed by using traditional cartesian Fourier transform (denoted as Cartesian cases) and hexagonal Fourier transform (denoted as Hexagonal cases), respectively. Note that the hexagonal Fourier transform does not change the mesh in physical space, *i.e.*, the computations are performed in a rectangle domain which can be rearranged to a hexagon under hexagonal periodic boundary conditions (see Fig. 3 for a sketch). The numerical resolutions for all cases are selected as the same 512^2. The time resolution is chosen with respect to the convergence criterion of Courant-Friedrichs-Lewy (CFL) number. All the cases are computed for 2×10^6 time steps to assure the time of evolution is long enough: it is observed that all cases converge to several large-scale vortices after this long time. We perform in total 160 cases, which means 80 Hexagonal cases and 80 Cartesian cases (see Table 1). Post-processings are performed based on these 160 cases.

We focus on the later evolution stage of 2D turbulence during which large-scale vortices dominate the system due to the backward energy transfer. As shown in Table 1, the cases are classified into four main categories respectively: fast formation of periodical

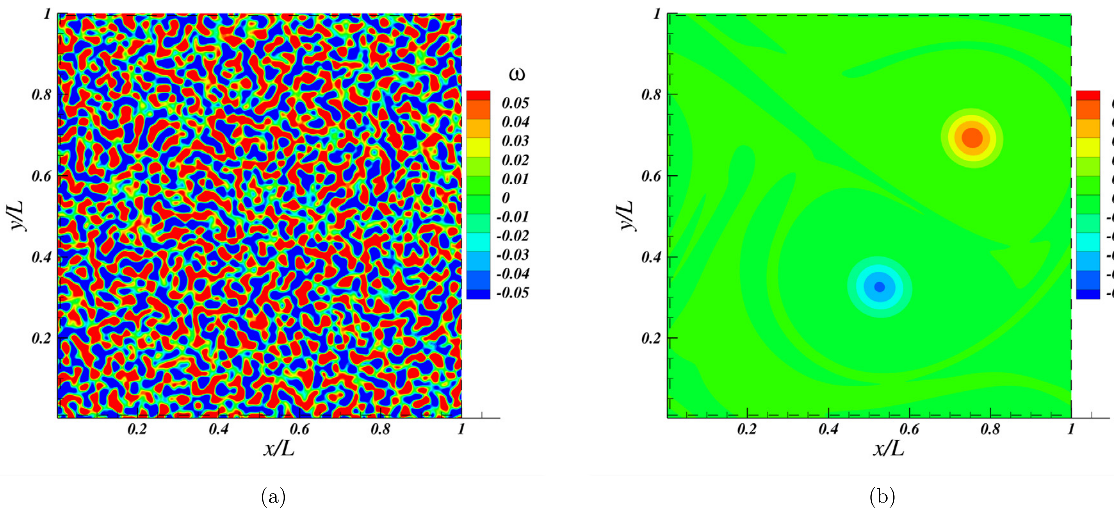

Fig. 1. Vorticity snapshots of a 2D freely decaying flow under square periodic boundary conditions. (a) Initial field. (b) After long-time evolution. Dashed lines indicate the boundary of a period. (For interpretation of the colors in the figure(s), the reader is referred to the web version of this article.)

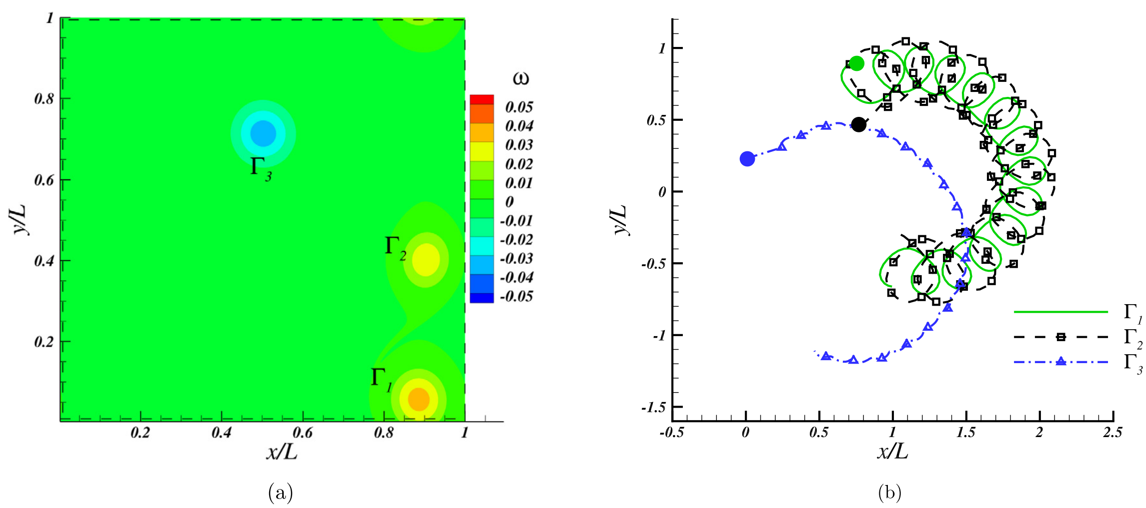

Fig. 2. (a) Vorticity snapshot of three-vortices coherent structure under square periodic boundary conditions, and (b) the trajectories of three vortices while maintaining the stable paired motion. The solid circles indicate the initial time of forming a system of three vortices.

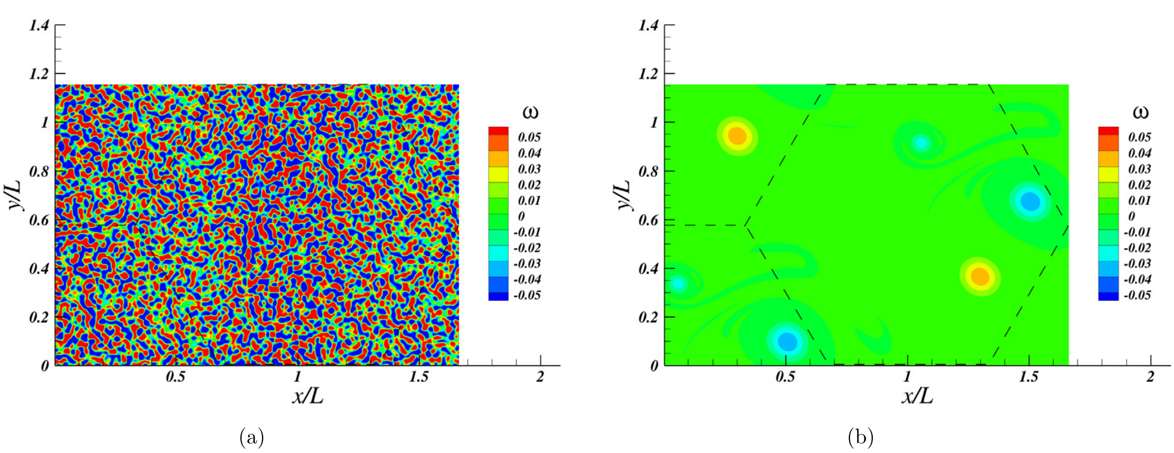

Fig. 3. Vorticity snapshots of three-vortices coherent structure under hexagonal periodic boundary conditions. The area in one hexagon is a period. (a) Initial field. (b) After long-time evolution. Dashed lines indicate the boundary of a period.

two-vortices coherent structure (denoted as Two-vortices), maintain of formation of periodical three-vortices coherent structure (denoted as Three-vortices), formation of periodical two-vortices coherent structure after maintaining periodical three-vortices coherent structure for long time (denoted as Three-vortices to Two-vortices), and formation of periodical two-vortices coherent structure after maintaining periodical four-vortices coherent structure for long time (denoted as Four-vortices to Two-vortices). As remarked in the previous subsection, the Two-vortices cases are trivial and hence not interesting. The following discussions will focus on the other motions.

2.3. Theoretical analysis

In 2D flow, the vorticity $\vec{\omega}$ is always a vector perpendicular to the flow plane. Considering the vorticity spectrum, we have

$$\hat{\vec{\omega}}(\vec{k}) = \mathcal{F}(\nabla \times \vec{v}) = i\vec{k} \times \hat{\vec{v}}(\vec{k}), \tag{1}$$

where $\hat{\vec{\omega}}$ is the vorticity spectrum, $\vec{k}$ is the wave vector, $\vec{v}$ is the velocity in physical space and $\hat{\vec{v}}$ is the velocity in spectral space. Taking $\vec{k}$ as $\vec{0}$ leads to

$$\hat{\vec{\omega}}(\vec{0}) = \vec{0} = \int\limits_{\vec{r}} \vec{\omega} d\vec{r}, \tag{2}$$

which indicates that the vorticity flux over a period of the present cases should be zero.

As shown in Figs. 1, 2 and 3, the vorticity is condensed in the vicinity of several large-scale vortices in long time. Theoretical analysis can approximately consider these large-scale vortices as point vortices. From Eq. (2) the summation of strength of these point vortices should be zero. For a system of three point vortices in a periodic parallelogram, the dynamics has already been studied systematically in Ref. [31]. In the following we will revisit the spirit of these theories of point vortices dynamics, in order to describe the physical quantities which will be used in the present post-processings.

As derived in Ref. [31], the dynamics of point vortices with zero net circulation in a periodic parallelogram can be represented by the following equations:

$$\begin{aligned}
\frac{d\overline{z_\alpha}}{dt} &= \frac{1}{2\pi i} \sum_{\beta=1,\beta\neq\alpha}^{N} \Gamma_\beta \left\{ \zeta(z_\alpha - z_\beta) + \left(\frac{\eta_1}{\omega_1} - \frac{\overline{\omega_1}\pi}{\omega\Delta} z_\beta + \frac{\pi}{\Delta}\overline{z_\beta}\right) \right\}, \\
\zeta(z;\omega_1,\omega_2) &= \frac{1}{z} + \sum_{(m,n)\in\mathbb{Z}^2, m\neq n} \left(\frac{1}{z-\Omega_{mn}} + \frac{1}{\Omega_{mn}} + \frac{z}{\Omega_{mn}^2} \right), \\
\Omega_{mn} &= 2m\omega_1 + 2n\omega_2, \\
\eta_1 &= \zeta(\omega_1;\omega_1,\omega_2), \\
\Delta &= 2i(\omega_1\overline{\omega_2} - \overline{\omega_1}\omega_2),
\end{aligned} \tag{3}$$

where N is the number of vortices in one period, z_α is the complex position of the αth vortex with $z_\alpha = x_\alpha + iy_\alpha$, Γ_β is the strength of the βth vortex, ω_1 and ω_2 are the complex half-periods, and ζ is the Weierstrass function. According to the expression of Weierstrass function, the motion of one vortex is influenced not only by the other vortices in the same period, but also by the vortices and its images in other periods. It can be deduced that for a system of two point vortices with zero net circulation in a periodic parallelogram, the properties of the motion is the same with the aperiodic case where there are only two vortices in an unbounded domain. However, for a system of three vortices, the case will be more complicated. In Ref. [31], by defining the parameter of strength and invariant of a three-vortices system with zero net circulation in a periodic parallelogram, there is

$$\begin{aligned}
&\frac{\Gamma_1}{\Gamma_3} = -\left(\frac{1}{2}+\gamma\right), \qquad \frac{\Gamma_2}{\Gamma_3} = -\left(\frac{1}{2}-\gamma\right), \\
&\Gamma_1 z_1 + \Gamma_2 z_2 + \Gamma_3 z_3 = Q + iP,
\end{aligned} \tag{4}$$

where γ is the parameter of strength and we only consider the case where $\Gamma_1 \geq \Gamma_2 > 0$ and $\Gamma 3 < 0$ without loss of generality. Q and P are the real and imaginary parts of the invariant of the three-vortices system in one period, respectively. Note that the values of Q and P are sensitive to the selection of the basic three vortices. In order to write the equations in a more compact form, one can map ω_1 to the real axis by rotating the coordinates. Accordingly, the equations write

$$\begin{aligned}
\frac{d\overline{z_1}}{dt} &= \frac{1}{2\pi i}\left[\Gamma_2\zeta(z_1-z_2) + \Gamma_3\zeta(z_1-z_3) + \frac{\eta_1}{\omega_1}(Q+iP) - \frac{P}{\Delta}\right], \\
\frac{d\overline{z_2}}{dt} &= \frac{1}{2\pi i}\left[\Gamma_1\zeta(z_2-z_1) + \Gamma_3\zeta(z_2-z_3) + \frac{\eta_1}{\omega_1}(Q+iP) - \frac{P}{\Delta}\right], \\
\frac{d\overline{z_3}}{dt} &= \frac{1}{2\pi i}\left[\Gamma_1\zeta(z_3-z_1) + \Gamma_2\zeta(z_3-z_2) + \frac{\eta_1}{\omega_1}(Q+iP) - \frac{P}{\Delta}\right].
\end{aligned} \tag{5}$$

Defining $Z = z_1 - z_2$, $X = -(Q+iP)/\Gamma_3$ and subtracting the first two equations of (5), the only independent equation for Z writes

$$\begin{aligned}
\frac{d\overline{Z}}{dt} = -\frac{\Gamma 3}{2\pi i}\Bigg[&\zeta(Z) + \zeta\left(X - \left(\frac{1}{2}+\gamma\right)Z\right) \\
&+ \zeta\left(X + \left(\frac{1}{2}-\gamma\right)Z\right)\Bigg],
\end{aligned} \tag{6}$$

then the equation of motion for z_1 can be written in terms of Z. Also, z_2 and z_3 can be easily deduced using Q, P and γ.

In Ref. [31], the analysis was focusing on Eq. (6) by choosing different parameter γ and by considering the problem as the advection of a passive particle by a certain set of point vortices. The analysis of the motion regimes of three vortices in a periodic parallelogram was based on the analysis of the streamline pattern of this passive particle. We remark that the two periodic boundary conditions that we use in DNS computation can also be both written in form of the periodic parallelogram. Specifically, the Hexagonal cases in the present contribution imply two periodical directions that constitute the two adjacent sides of parallelogram, *i.e.*, i and $\sqrt{3}/2 + i/2$ in the complex plane (denoted as $\vec{R}_1$ and $\vec{R}_2$ in Fig. 4(a) respectively).

In the present post-processing, identification of vortices is performed by searching for 2D extremums of vorticity magnitude above a threshold. The detailed procedure can refer to Ref. [9], while the threshold in the present paper is set as 20% of the maximal vorticity magnitude. The vortices are approximately considered as point vortices, while the strength for each vortex is calculated by integrating the vorticity in its vicinity. The vicinity for each vortex is determined by distinguish the minimum distance to one of the three vortices in one period and their images in the other eight periods around. Accordingly, at each instant, we can finally obtain the strength of three vortices with the total circulation to be zero. We remark that the present post-processing is an approximation by involving the concept of point vortices, but they are not exactly the same. A difference is that the strength calculated for each vortex will vary with the evolution of the present

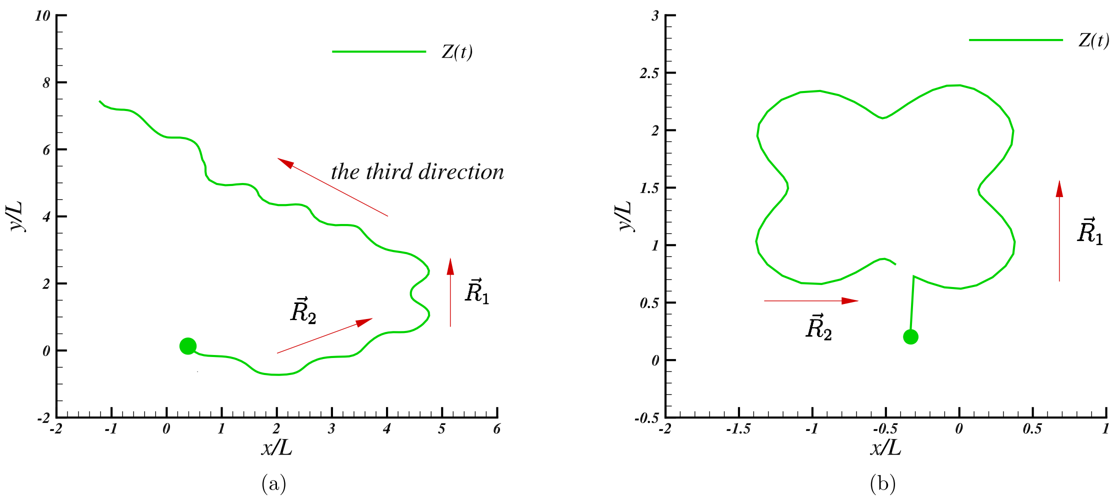

Fig. 4. Trajectory of $Z(t)$ with unbounded regime. (a) Hexagonal case No. 38. (b) Cartesian case No. 27.

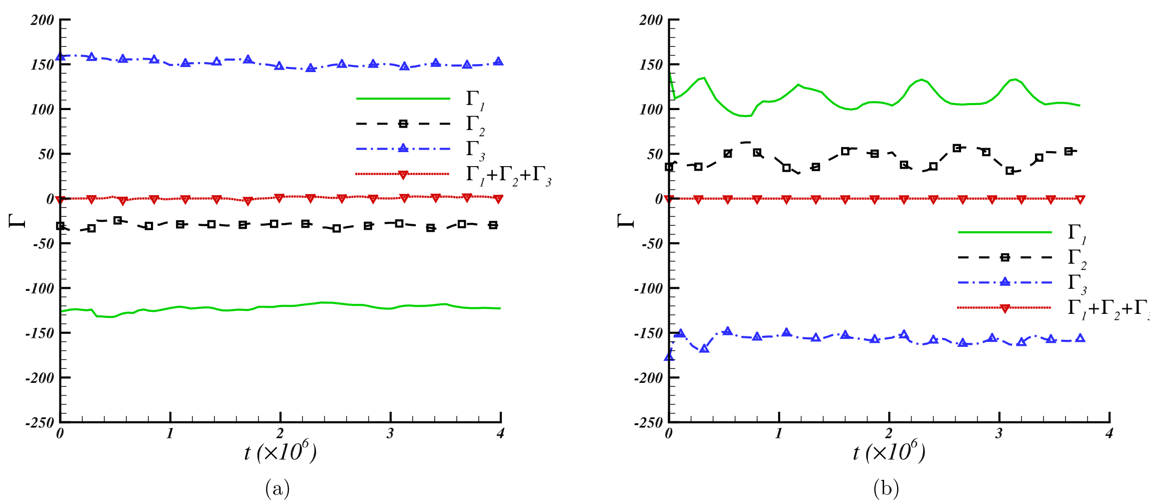

Fig. 5. Evolution of vortex strengths with unbounded regime. (a) Hexagonal case No. 38. (b) Cartesian case No. 27.

system, but for a point vortices system they are constant. As a result, the parameter γ will vary with time in the present DNS cases, which, by contrast, is a constant in a point vortices system.

In the following section, we will focus on the wandering motion with unbounded regime which was defined in Ref. [31] and compare the difference between the regimes occurred under different periodic conditions. Also, we will turn to the paired motions which are the most frequently observed bounded regimes in DNS cases.

3. Results

3.1. Analysis on the wandering motion with unbounded regime

As introduced in Eq. (6), the displacement between two vortices of the same sign, $Z(t)$, can be considered as a characteristic quantity for the dynamics of a three-vortices system. If the evolution of $Z(t)$ is unbounded, the situation was named as unbounded regime. A direct conclusion is that an initial set of three vortices in a period cannot always stay in a single period. As concluded in Ref. [31], when $\gamma = 0$, the only motion under the unbounded regime is the wandering motion, *i.e.*, $Z(t)$ migrates towards a typical direction. Under quadrate periodic conditions this direction can be one of the periodic directions; in a periodic parallelogram with two periodic directions that are not perpendicular, for example under hexagonal periodic conditions, this direction can be either one of the two periodic directions that defines the parallelogram, or the third direction defined by a linear combination of them.

In our DNS cases, wandering motions are also observed under both periodic conditions, but differences exist by comparing with point-vortex theories. Fig. 4 illustrates the difference in unbounded regime between two periodic conditions by giving two typical examples respectively. We remark that in each Cartesian DNS case with unbounded regime of three-vortices system, two periodic directions are the only typical directions for $Z(t)$. The third direction under hexagonal periodic conditions is marked in Fig. 4(a), by comparing with the two periodic directions $\vec{R}_1$ and $\vec{R}_2$. These directions are well consistent to the theoretical analysis in Ref. [31]. Differences exist between the present cases and the theoretical results of point vortices. As observed in Fig. 4, for both periodic conditions the direction in which the particle travels can change. This is contrary to Ref. [31], where wandering motions should always lead to migration in only one direction. There are two underlying reasons: *i*) the present vortices have vorticities distributed in a certain area and are not point vortices; *ii*) in the present cases the pre-condition of the theories of point vortices, $\gamma = 0$, cannot be satisfied. These facts mean that the dynamics of large-scale vortices can switch among different wandering motions of unbounded regimes, as observed in Fig. 4.

We also show the evolution of vortex strengths of these two cases in Fig. 5. The value of time on x-axis is normalized by using

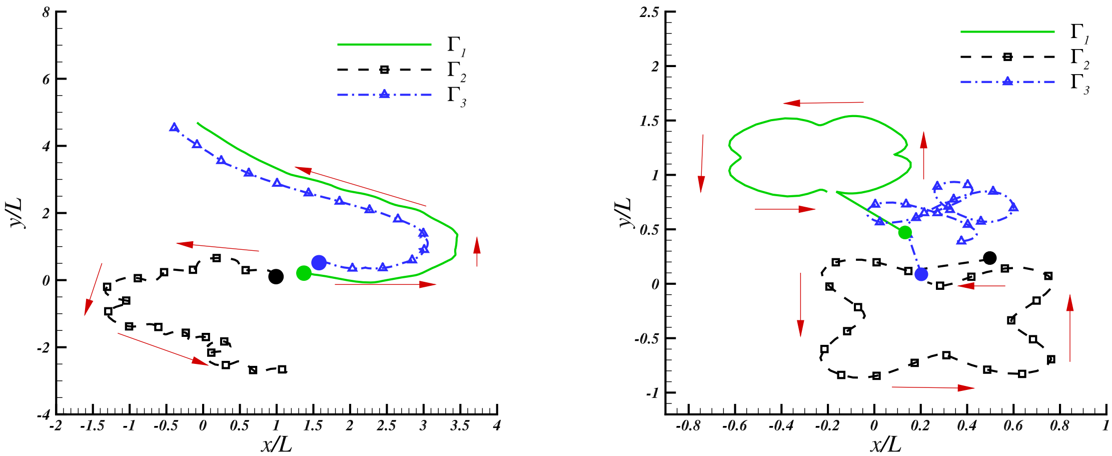

(a) (b)

Fig. 6. Trajectories of vortices with unbounded regime. (a) Hexagonal case No. 38. (b) Cartesian case No. 27.

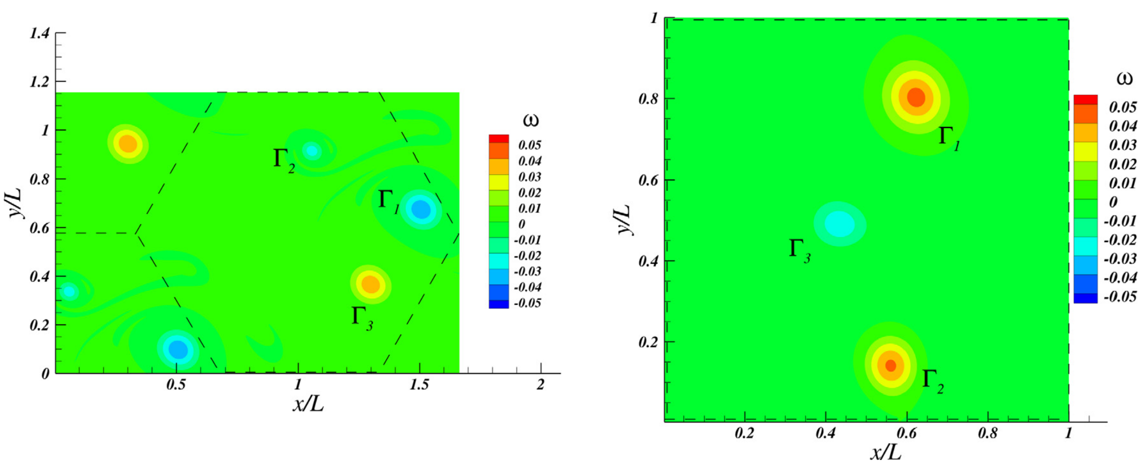

(a) (b)

Fig. 7. Vorticity snapshots of two cases with unbounded regime. (a) Hexagonal case No. 38. (b) Cartesian case No. 27.

a characteristic time $1/\max(|\Gamma_1|, |\Gamma_2|, |\Gamma_3|)$ at $t = 0$. It is clear that the total strength $\Gamma_1 + \Gamma_2 + \Gamma_3$ is very close to zero, which supports both our post-processing techniques and the zero-vorticity deduction in point-vortex theories [31]. The corresponding trajectories and vorticity snapshots are shown in Fig. 6 and 7 respectively. From Fig. 5(a) Γ_2 corresponds to the vortex which migrates among different periods in the Hexagonal case, while the vortex pair with strengths Γ_1 and Γ_3 remains always in a single period. It is interesting that Γ_2 is the weakest vortex among the three vortices in the Hexagonal case, and its location is far from the other two vortices as shown in Fig. 5(a). We remark that this phenomenon can be analogical to the physics of current flow: the weakest and smallest vortex is analogical to the outer-shell electron which can move among atoms, while the other two vortices are analogical to the proton and inner-shell electron. For comparison, in Fig. 5(b) there is no such kind of phenomenon.

Since in the present cases vortices cannot preserve constant strength, it is interesting to ask how much difference between DNS and point-vortex theories due to this variation of strength. In practice, we calculate the point-vortex evolution based on certain instants respectively by freezing the strengths of three vortices, and compare these analytical predicted trajectories with the real trajectories in Fig. 8. Coincidence can be observed in short term, while in long term they diverge. The corresponding temporal evolution of the distance (in practice, at each instant we calculate the mean value of the distances of three vortices) is shown in Fig. 9. Given a threshold distance value 10%, it is observed that the normalized time for reaching this threshold is of the magnitude of 10^5. This fact indicates that the point-vortex theories can be approximated used in a time interval of about 10^5. In order to give an intuitive view on this time length, we note that the time from a Gaussian initial field to a three-vortices state is about $6 \times 10^6 \sim 8 \times 10^6$.

3.2. Analysis on the paired motion with bounded regimes

According to Ref. [31], there are different motions in bounded regimes. From DNS results, it is observed that most cases with bounded regimes are paired motions, indicating that the paired motion represents the most important dynamics of the system of three vortices. In this section we will focus on two typical cases with almost similar initial vortex strengths, under different periodic conditions. Fig. 10 shows two examples with bounded regimes. Clearly the trajectories of $Z(t)$ are quasi periodic within a boundary. Fig. 11 further shows the evolution of vortex strengths. It is clear that each case is a system of three vortices, with two negative vortices of almost the same strength, and one positive vortex.

Fig. 12 shows the motion of each vortex. It is found that both cases evolve similarly, where Γ_3 corresponds to a quasi-straight translation, while the two negative vortices, Γ_1 and Γ_2, co-rotate

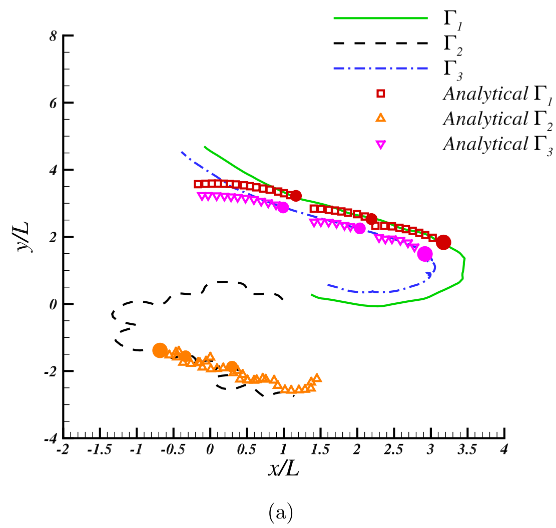

Fig. 8. Comparison of trajectories of vortices between DNS and analytical solutions by freezing the strength. Solid circles indicate different time instants of strength freezing. (a) Hexagonal case No. 38. (b) Cartesian case No. 27.

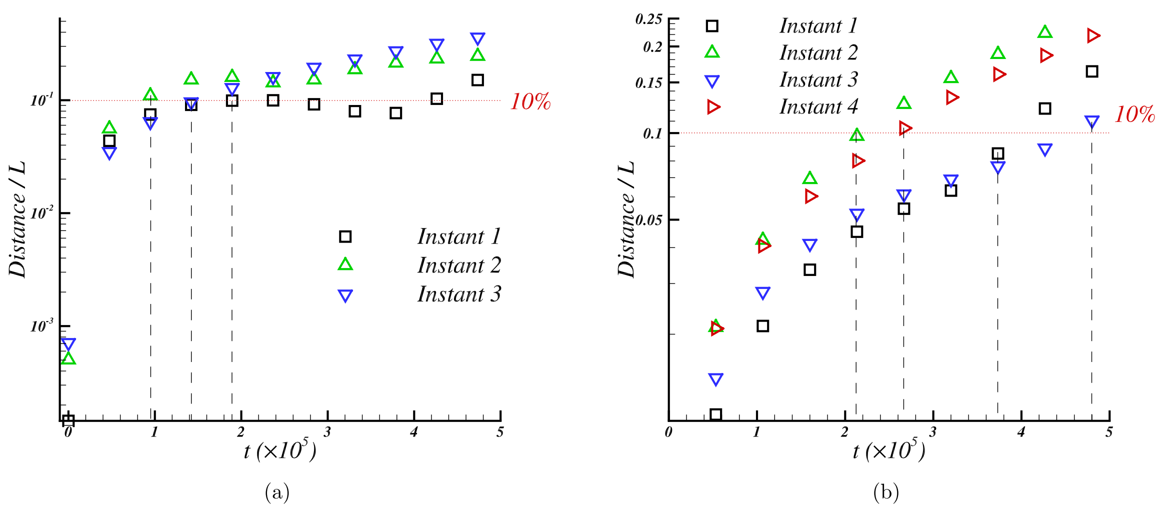

Fig. 9. Mean value of the trajectory distances of three vortices between DNS and analytical solutions by freezing the strength, at different time instants respectively. Domain period L is used for normalization. Horizontal dotted lines correspond to 10% distance, and vertical dashed lines indicate the time that the distance reaches 10%. (a) Hexagonal case No. 38. (b) Cartesian case No. 27.

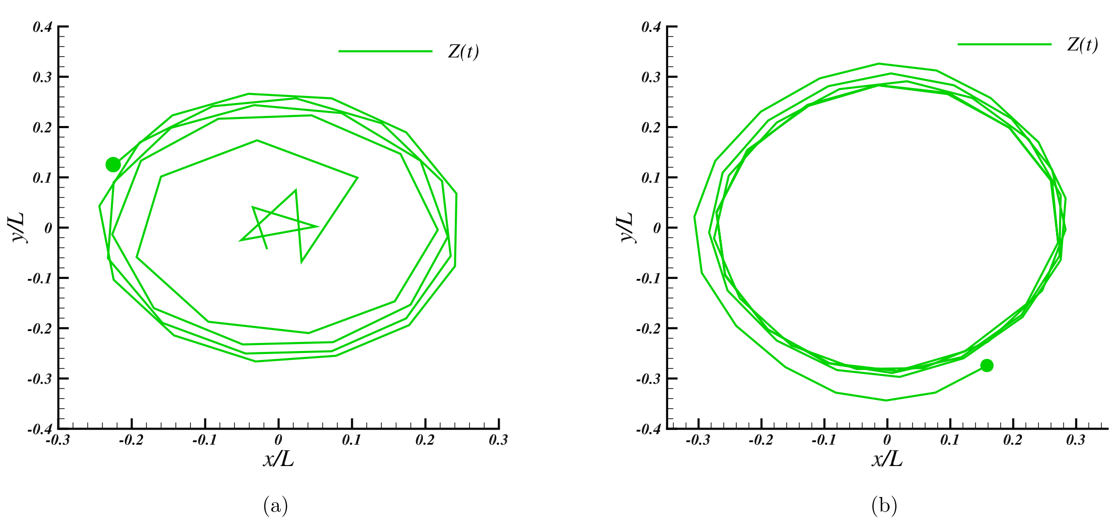

Fig. 10. Trajectory of $Z(t)$ with bounded regime. (a) Hexagonal case No. 6. (b) Cartesian case No. 16.

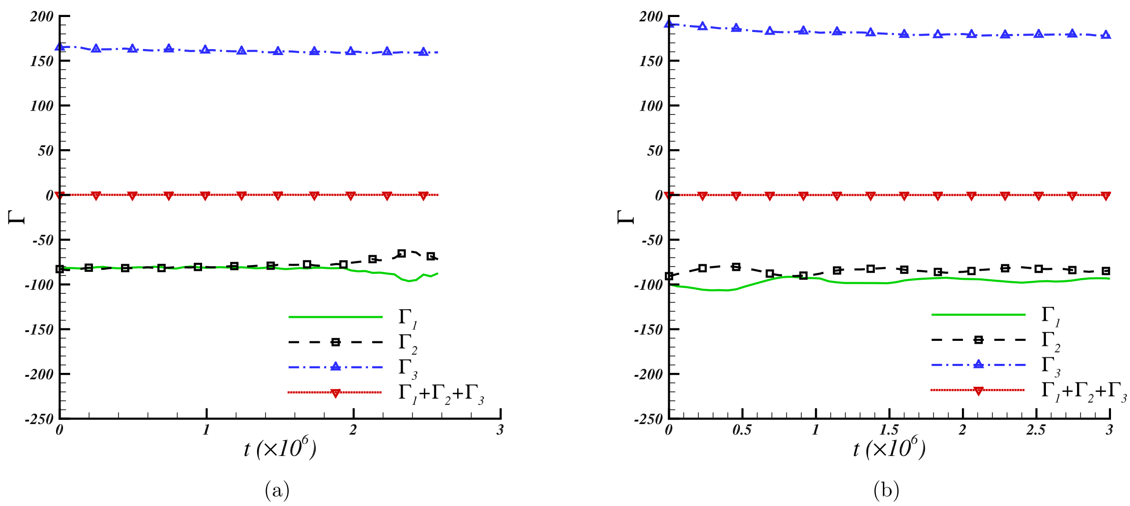

Fig. 11. Evolution of vortex strengths with bounded regime. (a) Hexagonal case No. 6. (b) Cartesian case No. 16.

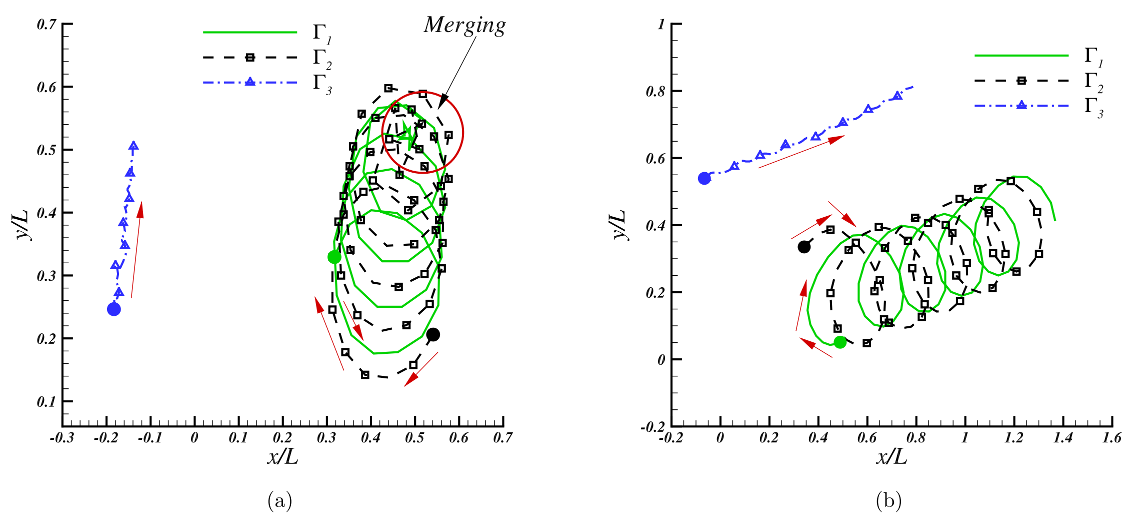

Fig. 12. Trajectories of vortices with bounded regime. (a)Hexagonal case No. 6. (b) Cartesian case No. 16.

and form a pair. This indicates that the paired motions, as described in Ref. [31] for point vortices, also exist in the real periodic 2D flows.

However, differences between Hexagonal case and Cartesian case can be observed in long time. As shown in Fig. 13, at initial time each of the two cases has three vortices in one period (marked with dashed lines), but after the same time ($t = 2.57 \times 10^6$) the Hexagonal case evolves to two vortices while Cartesian case remains three. We show accordingly the evolution of distances between each two vortices in Fig. 14. It is shown that in long time, the distance between Γ_1 and Γ_2 in Hexagonal case tends to zero, indicating that the two vortices merge to one vortex (it is also shown in Fig. 12(a) where the final merging stage is marked with a red circle). By contrast, in the present Cartesian case the vortices do not merge in the same time. We remark that this does not mean that the Hexagonal cases are always easier to merge vortices. In fact, from Table 1 the possibilities of merging, *i.e.*, the total numbers of "Three-vortices to Two-vortices" and "Four-vortices to Two-vortices", are almost the same for different periodic conditions (21 cases versus 22 cases). Here we are rather interested in searching for a physical quantity to represent this merging procedure more easily.

In order to describe the merging procedure, we introduce the skewness of vorticity (for 2D cases the only non-zero component of vorticity is in the direction perpendicular to the flow plane, denoted as ω), defined as

$$S_\omega = \frac{\langle \omega^3 \rangle}{\left(\langle \omega^2 \rangle\right)^{3/2}}, \tag{7}$$

where ensemble average $\langle\rangle$ is implemented by using spatial average. The ensemble average in denominator is proportional to the enstrophy, which is globally a quasi constant and only decays slowly due to viscosity [1,14]. For isotropic flows with reflection symmetry S_ω should be around zero. However, if we track the evolution of S_ω in different case, we can find that the plateaus and sudden changes correspond to different dynamics of vortices respectively. From the examples in Fig. 15, it is clear that the plateaus usually correspond to a quasi stable system of several large-scale vortices, while the sudden changes usually correspond to the procedure of vortex merging.

This phenomenon can be explained by expressing ω in spectral space. We can write

$$\omega(\vec{x}) = \sum_{\vec{k}\in\mathcal{K}} e^{i\vec{k}\cdot\vec{x}} a(\vec{k}) e^{i\phi(\vec{k})}, \tag{8}$$

where a is the amplitude and ϕ is the phase. $\mathcal{K}$ is the set of discrete wavevectors, which is related to the type of periodic condition and mesh resolution [20]. Derivations lead to

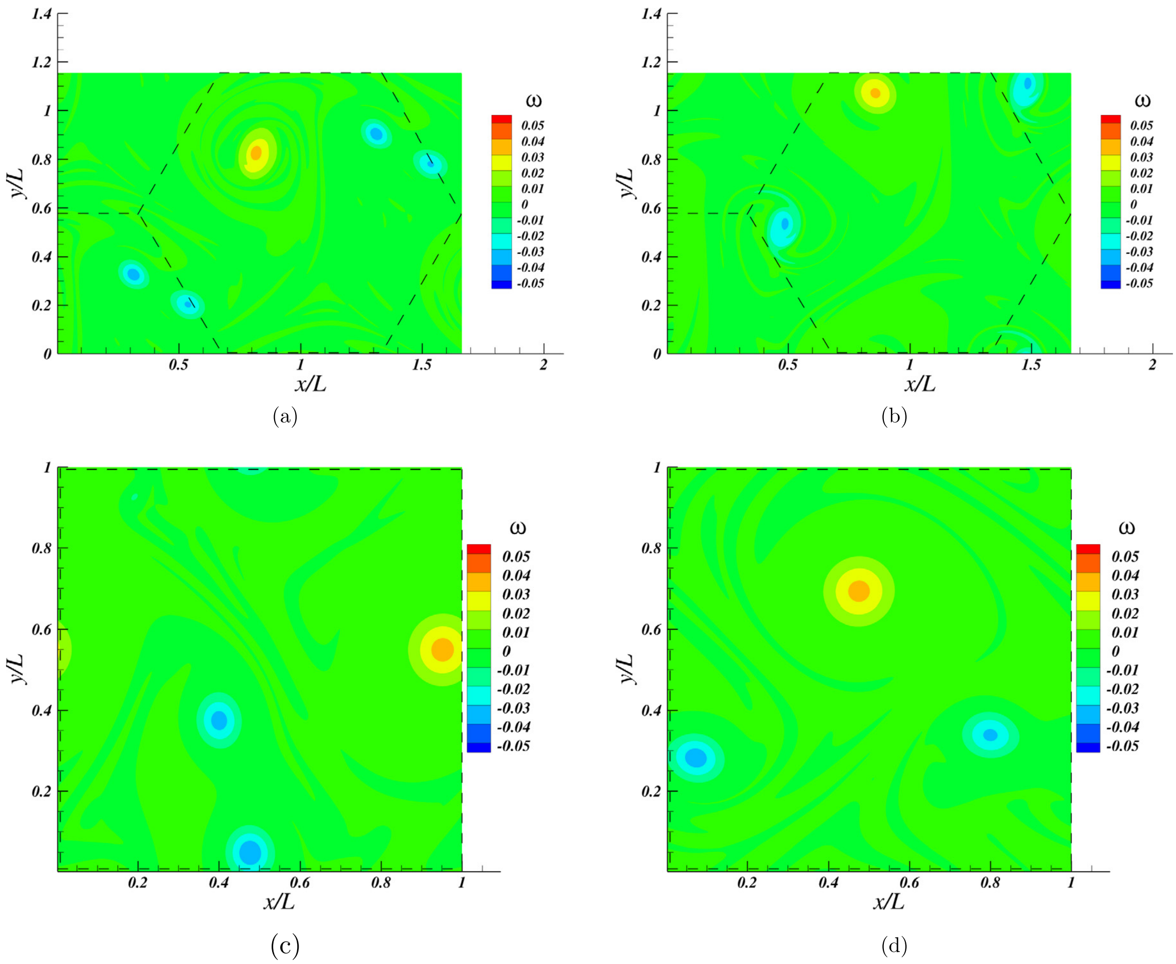

Fig. 13. Vorticity snapshots with bounded regime. (a) Hexagonal case No. 6, $t = 0$; (b) Hexagonal case No. 6, $t = 2.57 \times 10^6$; (c) Cartesian case No. 16, $t = 0$; (d) Cartesian case No. 16, $t = 2.57 \times 10^6$.

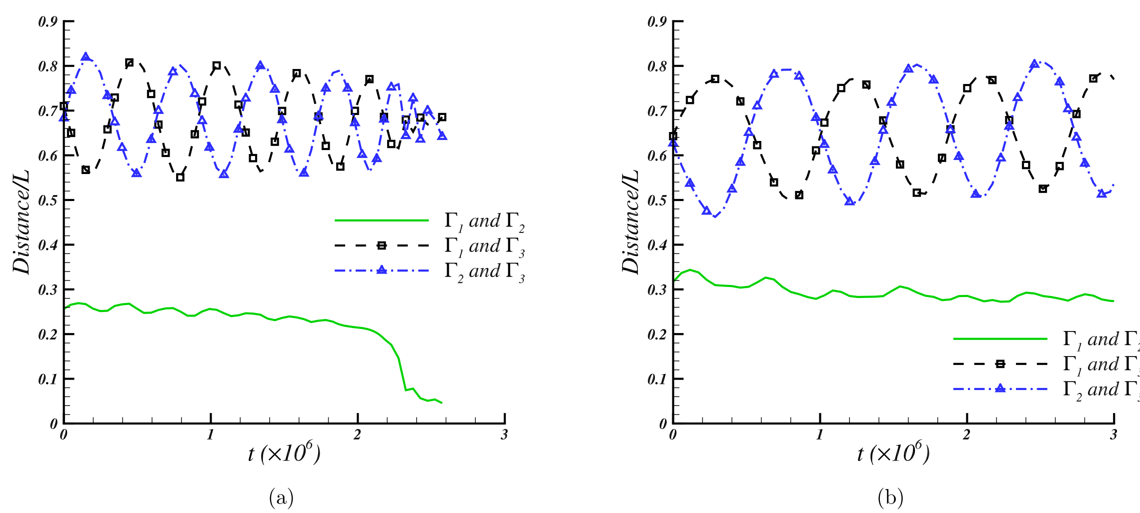

Fig. 14. Distance among three vortices with bounded regime. (a) Hexagonal case No. 6. (b) Cartesian case No. 16.

$$\omega^3(\vec{x}) = \sum_{\vec{k},\vec{p},\vec{q}} e^{i(\vec{k}+\vec{p}+\vec{q})\cdot\vec{x}} a(\vec{k})a(\vec{p})a(\vec{q}) e^{i(\phi(\vec{k})+\phi(\vec{p})+\phi(\vec{q}))}$$
$$= \sum_{\vec{m}} e^{i\vec{m}\cdot\vec{x}} \sum_{\vec{p},\vec{q}} a(\vec{m}-\vec{p}-\vec{q})a(\vec{p})a(\vec{q}) e^{i(\phi(\vec{m}-\vec{p}-\vec{q})+\phi(\vec{p})+\phi(\vec{q}))}. \tag{9}$$

The ensemble average corresponds to the $\vec{m} = \vec{0}$ mode, *i.e.*,

$$\left\langle \omega^3(\vec{x}) \right\rangle = \sum_{\vec{p},\vec{q}} a(-\vec{p}-\vec{q})a(\vec{p})a(\vec{q}) e^{i(\phi(-\vec{p}-\vec{q})+\phi(\vec{p})+\phi(\vec{q}))}. \tag{10}$$

Redefining $\vec{k} = \vec{p} + \vec{q}$, and using the conjugation symmetry condition $a(\vec{k}) = a(-\vec{k})$, $\phi(\vec{k}) = -\phi(-\vec{k})$, we write

$$\left\langle \omega^3(\vec{x}) \right\rangle = \sum_{\vec{k}=\vec{p}+\vec{q}} a(\vec{k})a(\vec{p})a(\vec{q}) \cos(\phi(\vec{p}) + \phi(\vec{q}) - \phi(\vec{k})). \tag{11}$$

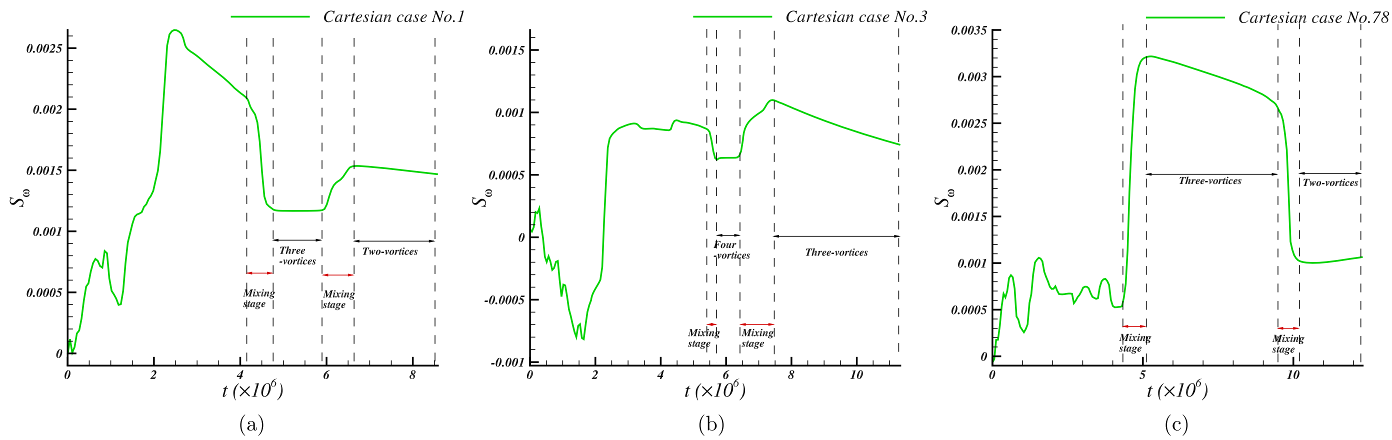

Fig. 15. Evolution of the skewness of vorticity with bounded regime. (a) Cartesian case No. 1; (b) Cartesian case No. 3; (c) Cartesian case No. 78.

Note that the pair of $(\vec{k}, \vec{p}, \vec{q})$ and $(-\vec{k}, -\vec{p}, -\vec{q})$ does not cancel each other. Approximately considering constant enstrophy, Eq. (11) is proportional to S_ω. Clearly, the value of S_ω is related to the interactions of triad wavevectors. As shown in Fig. 14(a), in procedure of vortex merging, the distances among vortices will rapidly change, indicating that Fourier component of new wavevectors arises. As a result, new triad interactions will generate, and from Eq. (11) S_ω should rapidly change. For comparison, a quasi stable system of several large-scale vortices corresponds to quasi stable triad interactions, therefore S_ω is accordingly quasi constant.

4. Conclusions

Most of existing studies on two-dimensional flows focus on the stage in which energies are contained at all scales, indicating the inter-scale transfer of energy and enstrophy. Few studies have focused on the late dynamics of large-scale vortices in periodic two-dimensional flows, which is investigated in the present contribution by using DNS results. Main conclusions are listed as follows.

1. The theories of point vortices can be also approximately employed for both quadrate and hexagonal periodic conditions. Specifically, freezing the vortex strengths and using point-vortex theories leads to less than 10% error of distance in an time interval of magnitude of 10^5. Conversely, our cases also support the theoretical solutions of point vortices with numerical facts. However, in real flows the dynamics can switch among different motions, which differs from the theory of point vortices. This is a result of the following effects: *i*) the size of vortices is not a point; *ii*) in real flows $\gamma \neq 0$ and is not constant.
2. As a special case of the wandering motions, the weakest vortex can migrate among different periods, with the other two vortices co-rotating. This phenomenon can be analogical to the physics of current flow.
3. The procedure that several vortices merge to one vortex, can be captured by tracking the sudden changes of the skewness of vorticity, since new wavevectors arise; by contrast, a quasi stable system of several large-scale vortices usually corresponds to quasi constant skewness of vorticity.

CRediT authorship contribution statement

J. Chai: Investigation, Validation, Software, Writing – original draft, Methodology. **L. Fang:** Supervision, Writing – review & editing, Funding acquisition, Conceptualization, Investigation, Methodology.

Declaration of competing interest

The authors declare that they have no known competing financial interests or personal relationships that could have appeared to influence the work reported in this paper.

Acknowledgement

Authors are grateful to Wouter Bos for providing the 2D turbulence code under square periodic conditions. This work is supported by the National Science Foundation in China (Grant No.s 11772032, 11572025).

References

[1] R.H. Kraichnan, Inertial ranges in two-dimensional turbulence, Phys. Fluids 10 (7) (1967) 1417–1423.
[2] A. Alexakis, L. Biferale, Cascades and transitions in turbulent flows, Phys. Rep. 767–769 (2018) 1–101.
[3] A.V. Pushkarev, W.J.T. Bos, Depletion of nonlinearity in two-dimensional turbulence, Phys. Fluids 26 (11) (2014) 115102.
[4] R.H. Kraichnan, D. Montgomery, Two-dimensional turbulence, Rep. Prog. Phys. 43 (5) (1980) 547–619.
[5] T.S. Lundgren, Y.B. Pointin, Statistical mechanics of two-dimensional vortices, J. Stat. Phys. 17 (5) (1977) 323–355.
[6] Y.B. Pointin, T.S. Lundgren, Statistical mechanics of two-dimensional vortices in a bounded container, Phys. Fluids 19 (10) (1976) 1459–1470.
[7] D. Montgomery, G. Joyce, Statistical mechanics of "negative temperature" states, Phys. Fluids 17 (6) (1974) 1139–1145.
[8] J.B. Taylor, M. Borchardt, P. Helander, Interacting vortices and spin-up in two-dimensional turbulence, Phys. Rev. Lett. 102 (2009) 124505.
[9] J.C. Mcwilliams, The vortices of two-dimensional turbulence, J. Fluid Mech. 219 (1990) 361–385.
[10] G.F. Carnevale, J.C. McWilliams, Y. Pomeau, J.B. Weiss, W.R. Young, Evolution of vortex statistics in two-dimensional turbulence, Phys. Rev. Lett. 66 (1991) 2735–2737.
[11] B.H. Burgess, D.G. Dritschel, R.K. Scott, Extended scale invariance in the vortices of freely evolving two-dimensional turbulence, Phys. Rev. Fluids 2 (2017) 114702.
[12] I.V. Kolokolov, V.V. Lebedev, Structure of coherent vortices generated by the inverse cascade of two-dimensional turbulence in a finite box, Phys. Rev. E 93 (2016) 033104.
[13] T. Gallay, C.E. Wayne, Global stability of vortex solutions of the wwo-dimensional Navier-Stokes equation, Commun. Math. Phys. 255 (1) (2005) 97–129.
[14] P. Tabeling, S. Burkhart, O. Cardoso, H. Willaime, Experimental study of freely decaying two-dimensional turbulence, Phys. Rev. Lett. 67 (27) (1991) 3772.
[15] T. Leweke, C.H.K. Williamson, Cooperative elliptic instability of a vortex pair, Phys. Fluids 360 (1998) 85–119.
[16] R.E. Robins, D.P. Delisi, Numerical study of vertical shear and stratification effects on the evolution of a vortex pair, AIAA J. 28 (4) (1990) 661–669.
[17] P. Meunier, S.L. Dizčs, T. Leweke, Physics of vortex merging, C. R. Phys. 6 (4) (2005) 431–450.
[18] J. Jiménez, H.K. Moffatt, C. Vasco, The structure of the vortices in freely decaying two-dimensional turbulence, J. Fluid Mech. 313 (1996) 209–222.

[19] C. Josserand, M. Rossi, The merging of two co-rotating vortices: a numerical study, Eur. J. Mech. B, Fluids 26 (6) (2007) 779–794.
[20] J. Chai, L. Fang, J.-P. Bertoglio, Reducing the background anisotropy by using hexagonal Fourier transform in two-dimensional turbulent flows, Comput. Fluids 210 (2020) 104671.
[21] P.K. Newton, Point vortex dynamics in the post-aref era, Fluid Dyn. Res. 46 (3) (2014) 031401.
[22] L.J. Campbell, J.B. Kadtke, Stationary configurations of point vortices and other logarithmic objects in two dimensions, Phys. Rev. Lett. 58 (7) (1987) 670–673.
[23] H. Aref, On the motion of three point vortices in a periodic strip, J. Fluid Mech. 314 (1996) 1–25.
[24] Y. Kimura, Chaos and collapse of a system of point vortices, Fluid Dyn. Res. 3 (1–4) (1988) 98–104.
[25] H. Aref, On the equilibrium and stability of a row of point vortices, J. Fluid Mech. 290 (1995) 167–181.
[26] A.I. Gudimenko, A.D. Zakharenko, Three-vortex motion with zero total circulation, J. Appl. Mech. Tech. Phys. 51 (3) (2010) 343–352.
[27] J.B. Weiss, J.C. Mcwilliams, Nonergodicity of point vortices, Phys. Fluids A, Fluid Dyn. 3 (5) (1991) 835–844.
[28] H. Aref, Motion of three vortices, Phys. Fluids 22 (3) (1979) 393–400.
[29] J. Tavantzis, L. Ting, The dynamics of three vortices revisited, Phys. Fluids 31 (6) (1988) 1392–1409.
[30] H. Aref, Stability of relative equilibria of three vortices, Phys. Fluids 21 (9) (2009) 094101.
[31] M.A. Stremler, H. Aref, Motion of three point vortices in a periodic parallelogram, J. Fluid Mech. 392 (1999) 101–128.
[32] E.A. Ryzhov, K.V. Koshel, Dynamics of a vortex pair interacting with a fixed point vortex, Europhys. Lett. 102 (4) (2013) 44004.
[33] K.V. Koshel, J.N. Reinaud, G. Riccardi, E.A. Ryzhov, Entrapping of a vortex pair interacting with a fixed point vortex revisited. I. Point vortices, Phys. Fluids 30 (9) (2018) 096603.
[34] J.N. Reinaud, K.V. Koshel, E.A. Ryzhov, Entrapping of a vortex pair interacting with a fixed point vortex revisited. II. Finite size vortices and the effect of deformation, Phys. Fluids 30 (9) (2018) 096604.
[35] R.S. Rogallo, Numerical experiments in homogeneous turbulence, NASA TM 81315, 1981.